Multifractal Analysis and Simulation of the Global Meteorological Network

Y. TESSIER, S. LOVEJOY,* AND D. SCHERTZER†

Collège Militaire Royal de St-Jean, Département de Physique, Richelain, Quebec, Canada

(Manuscript received 15 September 1993, in final form 30 March 1994)

ABSTRACT

Taking the example of the meteorological measuring network, it is shown how the density of stations can be characterized by multifractal measures. A series of multifractal analysis techniques are applied (including new ones designed to take into account the spherical geometry) to systematically test the limits and types of network multiscaling. These techniques start with a network density defined by grids or circles and proceed to systematically degrade their resolution (no a priori scaling assumptions are necessary). The multiscaling is found to hold over roughly the range 20 000 to 200 km (limited by the finite number of stations—here about 8000). Special attention is paid to qualitative changes in the scaling behavior occurring at very low and high density regions that the authors argue are associated with multifractal phase transitions. It is argued that the density was produced by a universal multifractal process, and the three corresponding universal multifractal parameters are estimated. The minimum and maximum orders of singularities present in the network are estimated, as well as the minimum- and maximum-order statistical moments that can be reliably estimated. The results are then used to simulate the effects of the finite number of stations on a network with the same statistical properties, and hence to quantitatively show that the observed breaks in the multiscaling can be accounted for by the finiteness. A growing number of geophysical fields have been shown to exhibit multiscaling properties over various ranges, and in this paper it is discussed how the bias introduced by the network clustering can be removed by new "multifractal objective analysis" procedures.

1. Introduction

The analysis of surface rainfall accumulations and other meteorological fields poses a basic geophysical problem: the inhomogeneity of the measuring networks that exhibit clustering over wide ranges of scale. Until recently, the problem was dealt with using geostatistical analysis techniques that were all predicated on the existence of well-defined spatial scales for the variability; that is, that the variability was restricted to a narrow range of scales. A new approach to the problem was made by Lovejoy et al. (1986a), who analyzed the distribution of the 9651 stations reporting to the World Meteorological Organization. Over the range 1–3000 km, it was found that the clustering occurs at all scales; the stations formed a geometrical fractal set. At first sight this result may seem surprising since the placement of the stations is the result of a hierarchy of decisions involving international, national, regional, and district agencies. However, these placement decisions are influenced by the position of landmasses, topography, demography, and economics, many of which have also been shown to respect scaling symmetries. For example, the earth's topography (including coastlines and distribution of islands) has long been known to exhibit scaling features [e.g., the algebraic falloff of the power spectrum, Venig-Meiniz (1951), Bell (1975), and others], and to be characterized by fractal structures (e.g., Richardson 1961; Mandelbrot 1967, 1975). The monofractal results reported in Lovejoy et al. 1986a [confirmed in studies of other networks, e.g., Korvin et al. (1990), Lovejoy and Schertzer (1988), Salvadori et al. (1994); see Korvin (1992) for a review] clearly showed that the placement decision-making process was sufficiently "multiscale" that it did not introduce an empirically detectable length scale in the range of approximately 1–3000 km. The new multifractal analyses discussed below show that this is also the case for the station density over the range of approximately 200–20 000 km.

Perhaps the most compelling reason to search for scaling regions and their limits is that the notion of scale invariance has now been developed as a symmetry principle (Schertzer and Lovejoy 1985; Lovejoy and Schertzer 1986); a priori, scaling must be our initial assumption. Only if and when specific scale-breaking mechanisms acting at well-defined spatial scales can be shown to exist can one justify the introduction of

---

[*] Current affiliation: Physics Department, McGill University, Montreal, Quebec, Canada.

[†] Current affiliation: Université Pierre et Marie Curie, Laboratoire de Météorologie Dynamique, Paris, France.

Corresponding author address: Dr. Yves Tessier, College Militaire Royal de St-Jean, Département de Physique, Richelain, Quebec J0J 1R0, Canada.
E-mail: tessier@cmr.ca

characteristic lengths. For example, due to the finite number of stations in the network Lovejoy et al. (1986) showed that the range of approximately 1–3000 km was roughly the maximum possible. These findings have already led to several applications: monofractal corrections to measurements to remove the bias introduced by the clustering (Lovejoy et al. 1986a,b), and the possibility of exploiting the scaling for "network optimization" (Nicolis 1993).

However, during the 1980s other important developments in scale invariance were made. Of special concern here was the realization that whereas the appropriate framework for studying scale-invariant geometric sets was fractals, for scale-invariant fields it was multifractals. Furthermore, "inhomogeneous" fractal sets (such as those associated with strange attractors) will generally define a series of fields (the density of points and its various powers) each of which will be characterized by a different fractal dimension (Grassberger 1983; Hentschel and Procaccia 1983; Schertzer and Lovejoy 1983, 1984). In the case of the network, this implies that the density of stations, pairs of stations, triplets of stations, etc., all had different fractal dimensions, a fact that was empirically substantiated (for the WMO network) in a report by Montariol and Giraud (1986). Since then, over various ranges of scale, many geophysical fields have been shown to be multifractal rather than monofractal, notably the topography (Lovejoy and Schertzer 1990; Lavallée et al. 1993), rain (Schertzer and Lovejoy 1985; Lovejoy et al. 1987; Lovejoy and Schertzer 1990, 1991; Gupta and Waymire 1990), cloud radiances (Gabriel et al. 1988; Tessier et al. 1993a), temperatures (Schmitt et al. 1992a), the wind field (Meneveau and Sreenivasan 1987; Chigirinskaya et al. 1994; Schmitt et al. 1992b, 1994), sea ice (Francis et al. 1994), the ocean surface (Tessier et al. 1993b), etc. In short, in geophysics, we are led from the idea of fractal networks intersecting fractal phenomena to that of multifractals detecting other multifractals.

Since the observed field will be a product of the network density and the actual field, multifractal corrections for the bias are conceptually straightforward, making the possibility of treating the sparse network problem in an entirely multifractal way quite attractive. Specific multifractal techniques for systematically correcting measurements for the sparseness: "multifractal objective analysis" (Tessier et al. 1993a; Salvadori et al. 1994; Tessier 1993) have already been proposed. However, before these can be taken too seriously, a complete empirical study of the multifractal properties of the network is needed including the range and type of scaling, the range of singularities present, and the existence of qualitative changes in the scaling for high and low densities. Such a study is now possible for the first time for several reasons: first, powerful new multifractal data analysis techniques (especially the probability distribution/multiple scaling technique, section 3, and the double trace moment technique, section 7) have been developed; second, there have been new theoretical advances including universal multifractals (Schertzer and Lovejoy 1987). Third is the quantification of qualitative changes in behavior associated with "multifractal phase transitions" (Schertzer et al. 1993; Schertzer and Lovejoy 1994, section 6). Finally, when the fundamental aspect of the network is considered to be the station density, then the data requirements are very large; a total of about 8000 stations turns out to be a very small number for this purpose. This leads us to extend correlation methods (section 5) in order to more intensively exploit the available data, but also to the necessity of performing multifractal simulations in order to obtain fuller confidence in our interpretation of the analyses (especially for the low-density regions, see section 8).

2. Monofractal analysis

Before turning to multifractal analyses, following Lovejoy et al. (1986a), we first repeat some of the monofractal analyses. This confirms the scaling of the slightly smaller network discussed here, which is of the 7983 synoptic stations that reported daily rainfall accumulation and whose data were archived at the National Meteorological Center (NMC) of the National Oceanographic and Atmospheric Administration (NOAA) during 1983 (Fig. 1). Examination of the figure shows that this distribution is far from being homogeneous: in fact—not surprisingly—the inhomogeneity of the network is highly correlated with landmasses and economics.

The fractal dimension D of a set can be estimated from the variation of the (average) number of points $\langle n(L) \rangle$ within a circle (or box) of size (L): $\langle n(L) \rangle \propto L^D$. If the circle is centered uniformly with respect to the set, D is the "box dimension" (an approximation to the Hausdorff dimension, usually considered the fractal dimension). If the circles are centered on points belonging to the fractal set, then D is the "correlation dimension." Because of the repeated sampling near clusters of points that the latter introduces, the box and correlation dimensions will not generally be identical (the latter is necessarily less than or equal to the former).

To apply these definitions, we must account for the curvature of the earth. Following Lovejoy et al. (1986a), we take $S(\theta)$ as the area of the spherical cap defined by two points subtending an angle θ at the earth's center (radius r) and then define the scale $L(\theta)$:

$$L(\theta) = \left[\frac{4}{\pi} S(\theta)\right]^{1/2} = \{2\pi r^2[1 - \cos(\theta)]\}^{1/2}. \quad (1)$$

This definition reduces to the usual great-circle distance ($=r\theta$) for small θ and has the property that the dimension of a network homogeneously distributed over the earth's surface network has the fractal dimen-

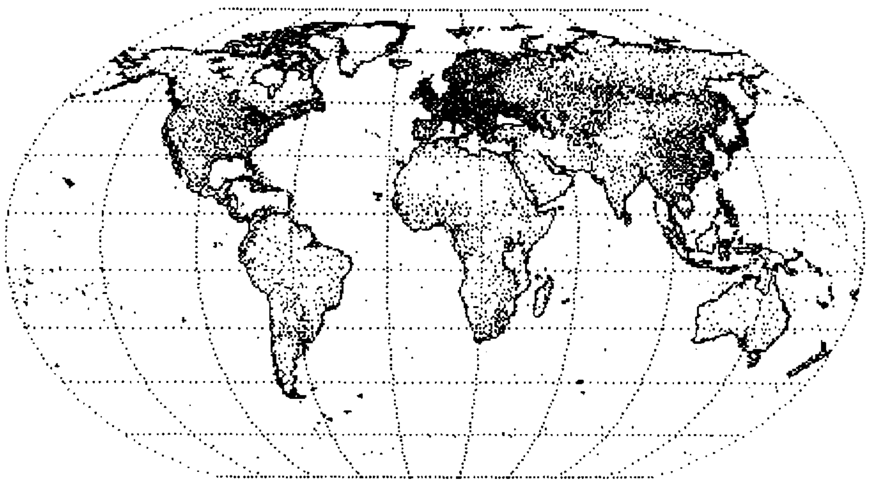

FIG. 1. Position of the stations reporting daily rainfall accumulations in 1983 that have been used in the analysis. Also plotted are the continent layouts for reference.

sion $D = 2$ as required. An estimate of the correlation dimension is obtained by determining the average number of pairs within a certain distance L (shown in Fig. 2). The scaling is found to hold quite well over the range of approximately 3–5000 km (a ratio of about 2000), which is nearly the maximum possible (the range is probably a bit wider since the minimum of about 3 km is the resolution of the data, possibly not the true minimum of the scaling). This maximum can be estimated by considering that if there are N stations in the network that $\langle n \rangle_{\max} = N/2 \approx 4000$, $\langle n \rangle_{\min} \approx 1/8000$, hence the range $\langle n \rangle_{\max} / \langle n \rangle_{\min} \approx N^2/2 = (L_{\max}/L_{\min})^D$; hence $L_{\max}/L_{\min} \approx 10\,000$.

The dimension obtained here is also almost the same as for the WMO network (approximately 1.79 compared to 1.75), which is not surprising since both networks follow similar geographic and economic constraint for their location and most of the stations are parts of both networks. We conclude that the slightly smaller network used here has comparable scaling properties to the WMO network.

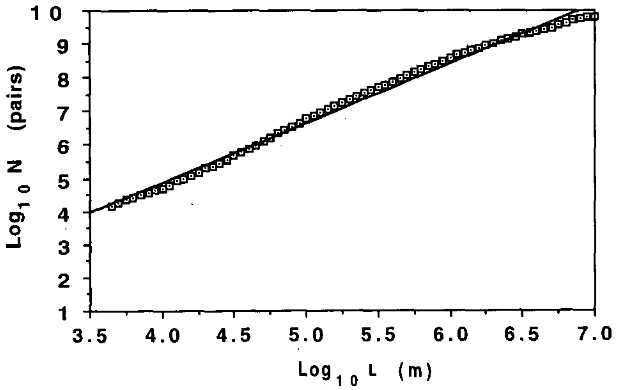

FIG. 2. Log of number of pairs of stations against the log of the distance between two stations. The solid line is the mean-square regression line fitting the data; the slope of this line gives the correlation dimension of the rain gauge network.

3. The probability distribution/multiple scaling technique

Monofractal techniques consider the measuring network as a geometric set of points. However, this only gives a very partial description since the clustering of the stations will not be the same as the clustering of the pairs, triplets, etc. Alternatively, more simply, a full characterization involves the density of stations, which is a field, and scaling fields are generally multifractals. We will now empirically show that the station density is approximately the density of a scale-invariant measure characterizing the actual station locations. This treatment of the stations is similar to that used in the characterization of strange attractors where the multifractal probability measures define the probability of finding the system in a given state. Whereas these measures are stable under a change of initial conditions, they are usually estimated by calculating the detailed distribution of points on a flow or mapping that may vary greatly from one initial condition to another. For general multifractals, an infinity of exponents (a scaling function) is needed to characterize the scaling behavior, one for each statistical moment.

A fundamental property of multifractal fields (Schertzer and Lovejoy 1987) is that the probability distribution is given by

$$\Pr(\rho_\lambda > \lambda^\gamma) \approx \lambda^{-c(\gamma)}, \qquad (2)$$

where λ is the resolution of the measure (i.e., the ratio of the external scale L to the measurement scale l; $\lambda = L/l$); ρ_λ is the intensity of the field measured at resolution λ (in this case the density of stations); and γ is the order of singularity corresponding to ρ_λ. The equality is to within slowly varying (logarithmic) prefactors. Here $c(\gamma)$ is the important codimension function that characterizes the sparseness of the γ-order singularities. When c is less than the dimension of space d (2 here), $D(\gamma) = d - c(\gamma)$ has a geometric interpretation as the corresponding fractal dimension. For example, the network codimension found in the previous section is $2 - 1.79 \approx 0.2$. The probability distribution/multiple scaling (PDMS) technique (Schertzer and Lovejoy 1989; Lavallée et al. 1991) uses histograms in order to directly estimate $c(\gamma)$. The method is based on Eq. (2) and consists in plotting logPr versus logλ for $\gamma = \log\rho_\lambda/\log\lambda$ constant. In this manner it accounts for the slowly varying prefactors in Eq. (2).

We chose to use grids such that each box has the same area. This is easily accomplished by partitioning the axis of the globe into slices of equal z (where z is the length of the projection of the slice onto the axis that goes from the center of the earth to the North Pole) so that the area of the intersection of each slice with the earth's surface will be the same. Finally, we partition the globe into slices of equal longitudes. The intersection of these two partitions gives a grid with elements ("boxes") of equal area (i.e., we have used a sinusoidal projection). Here, the finest resolution used was 512×512 since, as we shall see, this is already larger than the scaling range for the density (over a scale ratio of about 100). We also tried displacing the poles of this partition to check for possible north–south east–west dependence on the grid chosen due to the fact that the boxes do not all have the same shape (boxes near the poles are elongated in the north–south direction, whereas boxes near the equator are elongated in the east–west direction). No significant differences were observed. This coarse graining process is isotropic; in order to study the anisotropy, we need an anisotropic technique such as that discussed in the appendix or in Pflug et al. (1991, 1993).

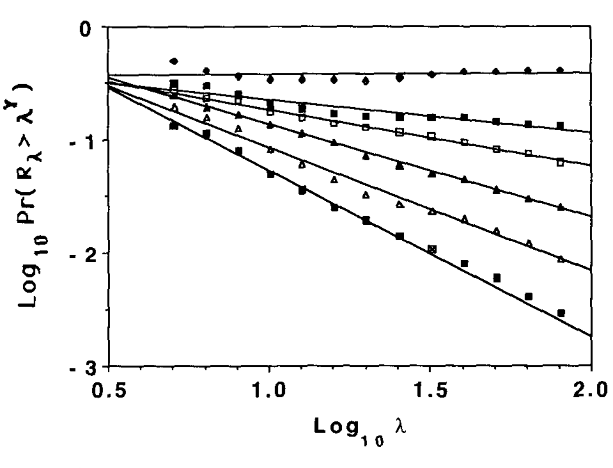

FIG. 3. PDMS analysis on the network. Log of the probability against the log of the scale ratio λ for different values of the singularity order γ (from top to bottom: $\gamma = 0.1$, 0.4, 0.5, 0.6, 0.7, and 0.8).

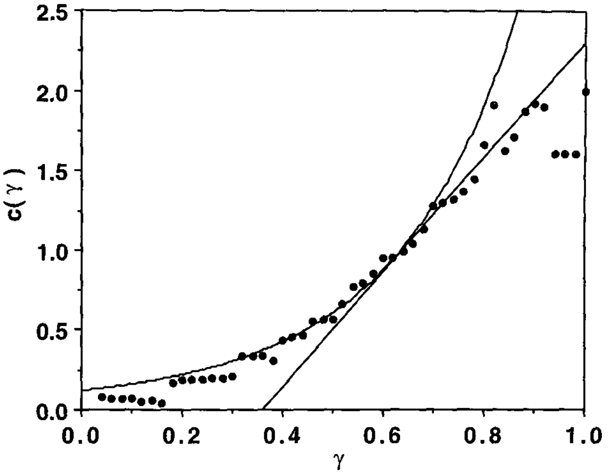

FIG. 4. The $c(\gamma)$ versus γ for the network deduced from the previous graph. Also shown is the theoretical bare curve with universal multifractal parameters $\alpha = 0.9$, $C_1 = 0.3$, and $H = 0$. The theoretical dressed curve is equal to the bare curve for $\gamma < \approx 0.6$ after which it follows the tangent (slope $q_D = 3.6 \pm 0.1$, also shown).

Using the grid, we then estimated the density of stations ρ_λ using the equation $\rho_\lambda = n/\lambda^{-2}$, where n is the number of stations in the grid element and λ^{-2} is the (nondimensionalized) area. The nondimensional normalized density obtained is then nondimensionalized by dividing by the mean density so that final normalized density has the property $\langle\rho_\lambda\rangle = 1$ (the angle brackets indicate ensemble average, here over all the grid elements; only one network is available). We then estimated the different probabilities using histograms; some of the logPr versus logλ curves are presented in Fig. 3. We see that good scaling is observed for $0 \leqslant \log\lambda \leqslant 2.0$ (i.e., from about 20 000 to 200 km). The fact that over this scaling regime the slopes are not the same indicates that the network density is multifractal rather than monofractal. The corresponding multifractal codimension function $c(\gamma)$ is obtained from the slope of these lines and is shown in Fig. 4. One reason for this more limited range of scaling compared to the monofractal analysis of section 2 is that by using boxes, we have $(L_{\max}/L_{\min})^D \approx N$ rather than $N^2/2$ as for the correlation method; hence $L_{\max}/L_{\min} \approx 8000^{1/1.8} \approx 150$. In section 5, we attempt to improve on this by using pairs of stations to estimate the histograms.

Having established the multiscaling of the station density, we now consider the possible behavior of $c(\gamma)$. After a considerable period of debate (Kolmogorov 1962; Yaglom 1966; Mandelbrot 1974), it has become clear (Schertzer and Lovejoy 1987, 1989, 1991; Brax and Peschanski 1991) that multifractal processes possess stable and attractive universality classes. This means that if the stations distribution arises from a scaling nonlinear process, then under fairly general conditions, we expect $c(\gamma)$ to have the following form involving only three basic parameters:

$$c(\gamma - H) = \begin{cases} C_1\left(\dfrac{\gamma}{C_1\alpha'} + \dfrac{1}{\alpha}\right)^{\alpha'}, & \alpha \neq 1 \\ C_1\exp\left(\dfrac{\gamma}{C_1} - 1\right), & \alpha = 1 \end{cases} \qquad (3)$$

where

$$\frac{1}{\alpha} + \frac{1}{\alpha'} = 1,$$

and $0 \leqslant \alpha \leqslant 2$ is the Levy index of the generator. It characterizes the degree of multifractality of the field (0 for a monofractal and 2 for a lognormal generator), C_1 is the codimension of the mean and quantifies the sparseness of the mean field, and H is the degree of nonconservation of the field (see section 8). Note that $c(\gamma)$ has the special property of having a fixed point $c(C_1 - H) = C_1$, and at the fixed point, $c'(C_1 - H) = 1$.

To test the universality hypothesis and to estimate the different universal multifractal parameters we tried to directly fit Eq. (3) with the data of Fig. 4. Nonlinear curve-fitting algorithms such as the Levenberg–Marquant (see Press et al. 1992) or the simplex method (see Griffiths and Hill 1985) failed badly to converge to a solution. The regressions problems are due to the high degree of correlation between the parameters and the limited range of γ's accessible to our analysis. The theoretical curve shown on the same figure was calculated using the parameters obtained with the double trace moment technique described in section 7; $\alpha \approx 0.9$, $C_1 \approx 0.3$, $H \approx 0$.

A few characteristics of Fig. 4 are worth mentioning. First, as expected from the results of the previous section, the minimum codimension $c(\gamma_{\min}) \approx 0.2$ corresponds to the codimension of the network (section 2), which is in good agreement with Fig. 4, with $\gamma_{\min} \approx 0.3$. Turning to the large γ region, we note that for values of $\gamma > \gamma_D \approx 0.6$, instead of following universal relations (the curved line) we observe qualitative change in behavior; a roughly linear behavior with slope $q_D \approx 3.6 \pm 0.1$. As we shall see in section 6 this qualitative change in behavior is a theoretically expected "multifractal phase transition." Another characteristic of Fig. 4 worth noting for future reference is the value $\gamma_{d,s}$, which is the maximum attainable singularity with a single two-dimensional sample and satisfies $c(\gamma_{d,s}) = 2$ (the dimension of the surface); by inspection, we find $\gamma_{d,s} \approx 0.8$ (see section 6). Finally, by using the fixed point property of Eq. (3), we can graphically estimate $H \approx 0.0$ [see Lovejoy and Schertzer (1990) for a discussion of this technique; we have used the above value $C_1 = 0.3$ since the curve is very noisy for the corresponding low γ's].

4. Trace moments

An alternative to the probability distribution description presented in section 3 is the use of statistical moments. Both descriptions are equivalent and related by a Legendre transform (Parisi and Frisch 1985). If we express the scaling of the moments by

$$\langle \rho_\lambda^q \rangle \sim \lambda^{K(q)}, \qquad (4)$$

where $K(q)$ is the moment scaling function, it is given by

$$K(q) = \min_\gamma[q\gamma - c(\gamma)];$$

$$c(\gamma) = \min_q[q\gamma - K(q)], \qquad (5a)$$

which leads to a one-to-one relation between singularities and moments:

$$q = c'(\gamma); \quad \gamma = K'(q). \qquad (5b)$$

Using Eq. (5a), $K(q)$ we obtain the following universal relation equivalent to Eq. (4):

$$K(q) + qH = \begin{cases} \dfrac{C_1}{\alpha - 1}(q^\alpha - q), & \alpha \neq 1 \\ C_1 q \log(q), & \alpha = 1. \end{cases} \qquad (6)$$

The trace moment technique (Schertzer and Lovejoy 1987) estimates $K(q)$ by generalizing the (deterministic) partition function approach of Halsey et al. (1986); to deal with stochastic multifractal processes, it generally involves ensemble averaging, although here we analyze a single network so the partition function and trace moment will be identical. Just as with the PDMS method, no a priori assumptions about the scaling of the process are necessary; the accuracy of the scaling is determined by the goodness of fit of the log–log regressions of moment versus scale.

To estimate the statistical moments of order q at different resolutions we use the same projection as described in section 3. At a given box size λ for a series of values of q we estimate

$$\langle \rho_\lambda^q \rangle \propto \frac{1}{N_b(\lambda)} \sum_{i=1}^{i=N_b} \left(\frac{n_i}{\lambda^{-2}}\right)^q, \qquad (7)$$

where the sum is over the N_b boxes needed to disjointedly cover the set (indexed by i). Then we repeat the procedure for different box sizes λ. Figure 5 shows the results of this analysis on a 512 × 512 grid for various values of q. We can see that as expected from analysis of the histograms, the scaling is observed in the range $0 \leqslant \log\lambda \leqslant 2.0$ (approximately 20 000 to 200 km: roughly the same as before). From the slopes of the curves of Fig. 5 in the scaling region we can deduce the $K(q)$ function (Fig. 6).

Once again we used the Levenberg–Marquant method to fit the $K(q)$ function to the form given by Eq. (6) (by using the portion of the curve expected to follow this relation, $q < q_D$, see below). We obtained

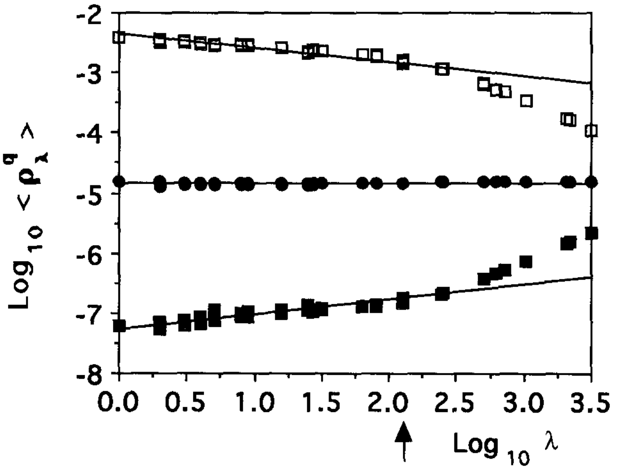

FIG. 5. Log of the statistical moments against log of the scale ratio λ for the network for moments of order $q = 0.5$ (empty squares), $q = 1.0$ (filled circles), and $q = 1.5$ (filled squares). The arrows indicate the limits of the scaling region. Here $\lambda = 1$ corresponds approximately to 20 000 km.

$\alpha \approx 0.9$, $C_1 \approx 0.3$, and $H \approx 0$ but with 95% confidence interval on α larger than the allowed range. This is actually fairly close to the values estimated by the more robust technique described in the next section. The theoretical curve for these parameters is also shown in Fig. 6 (using $\alpha = 0.9$, $C_1 = 0.3$, and $H = 0$ from section 8). Once again, for $q > q_D \approx 3.6$, we observe a linear behavior. This change is because the universal relations [Eqs. (3) and (6)] are followed only for a finite range of q and γ; we have multifractal phase transitions (section 6). For low q ($q_{\min} \approx 0.7$), we also observe a linear behavior with intercept at $-c(\gamma_{\min}) \approx -0.35$ [see Eq. (8)]. This change in the second derivative of K is also a phase transition and can be readily understood from Eq. (5a) by considering the effect of a restriction on the available γ's. In this case, then the minimization in Eq. (5a) will be over a finite range of γ's, and we anticipate that they will lead to regions with linear behavior in $K(q)$ [the $\gamma_{\min}$ will dominate all estimates of moments less than $q_{\min} = c'(\gamma_{\min})$]. Specifically, if due to the finite number of stations, there is a minimum nonzero $\rho_{\lambda_{\min}}$, then $\gamma_{\min} = \log\rho_{\lambda_{\min}}/\log\lambda$ thus implies $\gamma > \gamma_{\min}$, and hence for $q < q_{\min} = c'(\gamma_{\min})K(q)$ is linear (with slope $\gamma_{\min} \approx 0.3$, close to the value estimated in section 3). For $q < q_{\min}$, we obtain

$$K(q) = \gamma_{\min}(q - q_{\min}) + K(q_{\min}) = \gamma_{\min}q - c(\gamma_{\min}); \qquad q < q_{\min}. \quad (8)$$

In section 6 we discuss this phenomenon in more detail.

5. Correlation method

We have seen that our statistics are limited due to the fact that as far as estimating densities of stations is concerned, the 8000 available stations is a small number. Furthermore, we obtained a slightly different but more limited scaling range of approximately 200 to 20 000 km for the density compared to about 3 to 5000 for the individual stations; this is at least partly due to the fact that whereas the correlation method involves approximately $N^2/2$ pairs, the grid methods involve only N points. This suggests the possibility of using a variation on the trace moments technique obtained by an extension of the method used to estimate the correlation dimension: the correlation method. Of course the disadvantages are that while it is true that there are many more point pairs than points, many are correlated, and the method is computationally more demanding. It also will involve a bias since it investigates regions around points that are part of the fractal set (generally one is more likely to find points belonging to the set near points already part of the set and this bias must be removed).

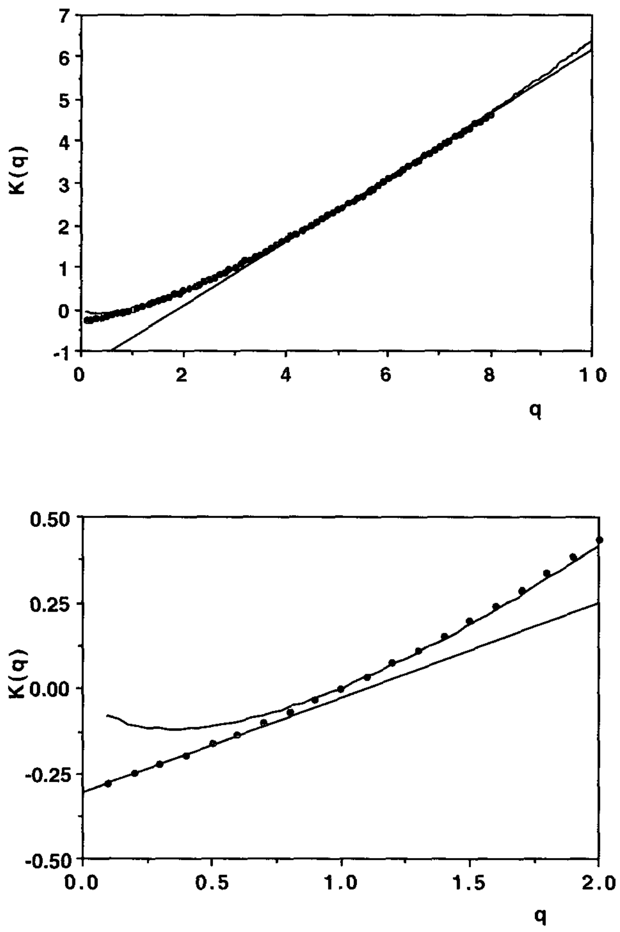

FIG. 6. The scaling exponent $K(q)$ versus q for the regular grid method with the fitting curve having scaling parameters $\alpha = 0.9$ and $C_1 = 0.3$. On the top figure the asymptotic linear region (after a multifractal phase transition) is fitted to a straight line of slope $\gamma_{d,s} = 0.7 \pm 0.1$. On the bottom figure, the linear region for small q is fitted to a straight of slope $\gamma_{\min} = 0.3 \pm 0.1$.

We consider each station in turn and calculate the distance [defined by Eq. (1)] to successively all other stations. We then calculate histograms of the number of stations in logarithmically spaced annuli surrounding each station. For convenience, ten annuli per order of magnitude were used. Starting from the smallest annuli, we integrated, determining the total number of stations within the corresponding circles. From these histograms we can calculate the moments $\langle \rho_\lambda^q \rangle$ for scale λ. By successively considering each station as a center, we can build up histograms at each distance of the total frequency of occurrence of a given number of stations. Before doing so we must correct for the bias introduced by using the stations' nonuniformly randomly placed centers in order to determine the equivalent of an analysis on a regular grid. We know that there are $n(n-1)/2 \sim n^2$ pairs in balls of radius λ with n points; this will lead to more robust statistics and this tells us that the first correction we have to do is to correct for the oversampling in regions with many stations; they will each be sampled approximately n times too often.

To quantify this precisely, consider a box size λ. We observe $N_\lambda(n)$ boxes with n stations. With the correlation method we will perform the same observation approximately n times (once with each of the stations as centers), obtaining the frequency $N_{\lambda\mathrm{cor}}(n)$. Hence the corresponding frequency that would have been observed on a regular grid is given by

$$N_\lambda(n) \approx \frac{N_{\lambda\mathrm{cor}}(n)}{n}. \tag{9}$$

Denoting the probability of a box at scale λ having n points by $p_\lambda(n)$, we have

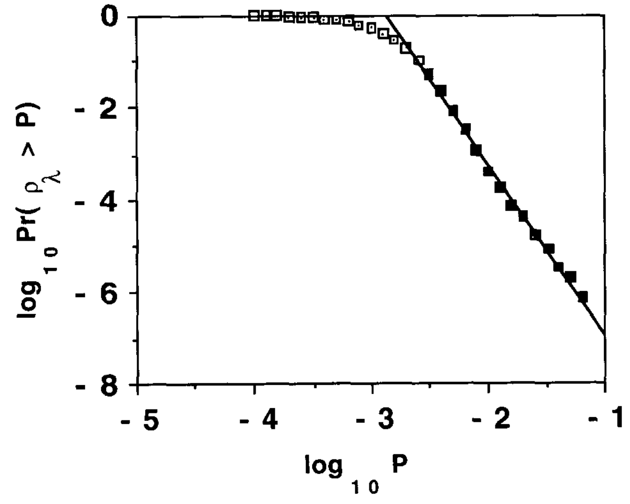

FIG. 7. Log of the probability of finding a density of station greater than ρ in a circle of 800 km against $\log\rho$. The asymptotic slope gives directly the exponent q_D that we estimate to be 3.7 ± 0.1.

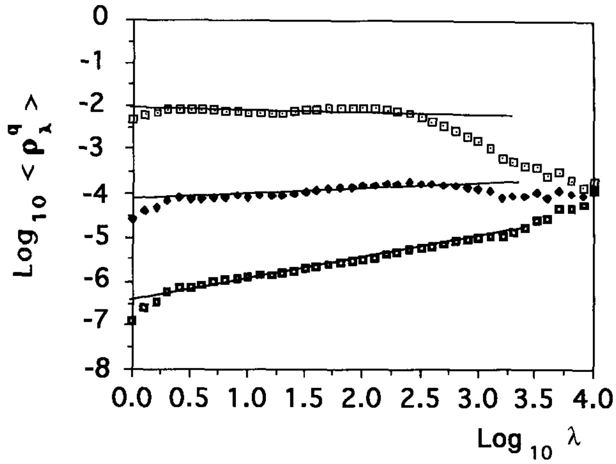

FIG. 8. Log of the statistical moments against $\log\lambda$ for the network using the correlation method for moments of order $q = 0.5$ (empty squares), $q = 1.0$ (filled diamonds), and $q = 1.5$ (filled squares). Here $\lambda = 1$ corresponds approximately to 20 000 km.

$$p_\lambda(n) = \frac{N_\lambda(n)}{N_{\lambda\mathrm{tot}}}, \tag{10}$$

where $N_{\lambda\mathrm{tot}} \approx \lambda^D$ is the total number of nonempty boxes at resolution λ (D is the box dimension, about 1.8 here). Recalling that $\rho_\lambda \propto n\lambda^2$, we obtain

$$\langle \rho_\lambda^q \rangle \propto \lambda^{2q-D} \sum_{n=1}^{N_{\lambda\mathrm{tot}}} N_{\lambda\mathrm{cor}}(n) n^{q-1}. \tag{11}$$

With this method we obtained the $\log\langle \rho_\lambda^q \rangle$ versus $\log\lambda$ curves shown in Fig. 8. From this we deduce that the scaling region is approximately $0.4 \leqslant \log\lambda \leqslant 2.2$, so the scaling range reaches slightly larger λ for the correlation method (note, however, that the definition of scale is slightly different in both cases). From these we deduce the $K(q)$ curve shown in Fig. 9. We fitted the $K(q)$ functions to the form given by Eq. (6) by the Levenberg–Marquant method and we obtained $\alpha \approx 1.0$, $C_1 \approx 0.2$, and $H \approx 0.1$ with once again very large confidence intervals.

With this method we estimate from the linear part of the low-q region that phase transitions occur for $q_{\min} = 0.7 \pm 0.1$ ($\gamma_{\min} = 0.26$), and from the intercept at $q = 0$, we deduce $c(\gamma_{\min}) \approx 0.28$. At large q, the slope of the asymptotic region gives us $\gamma_{d,s} = 0.82 \pm 0.05$ [see the next section, Eq. (15)]. We can see from Figs. 6 and 9 that as expected because of its somewhat more intensive sampling of the low-density regions, in the low-q region the correlation method is slightly more sensitive to low-order moments, yielding lower $\gamma_{\min}$, $q_{\min}$ (see Table 1 for an overall comparison). On Fig. 10, we see that we get similar results for both methods. Comparison of the grid and correlation method shows that the effective increase in the accessible range of γ is small: roughly, $\gamma_{\min}$ is reduced from 0.35 to 0.26,

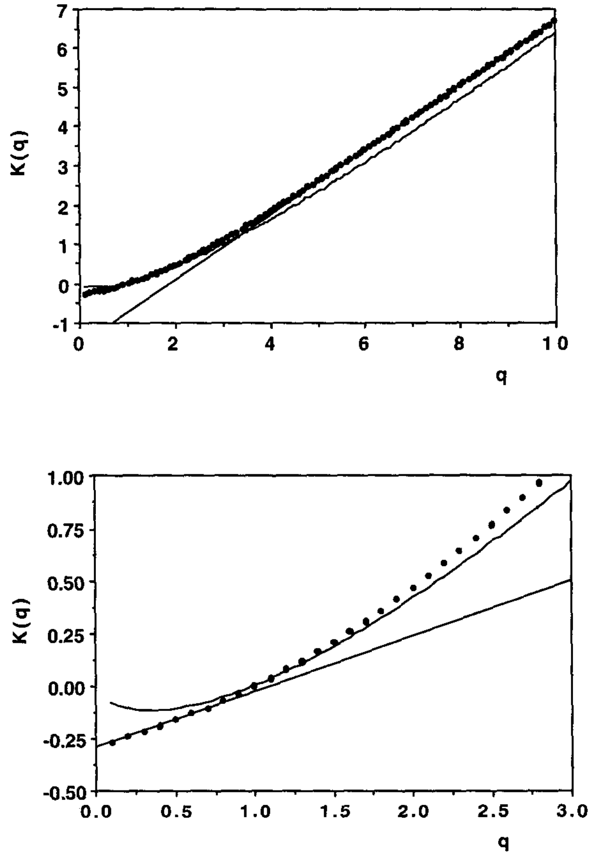

FIG. 9. The scaling exponent $K(q)$ versus q for the correlation grid method with the fitting curve having scaling parameters $\alpha = 0.9$ and $C_1 = 0.3$. On the top figure the asymptotic linear region (after a multifractal phase transition) is fitted to a straight line of slope $\gamma_{d,s} = 0.8 \pm 0.1$. On the bottom figure, the linear region for small q is fitted to a straight of slope $\gamma_{\min} = 0.2 \pm 0.1$.

and the maximum ($\gamma_{d,s}$) increases slightly from 0.7 to 0.8.

6. Multifractal phase transitions

We have already noted the appearance of various linear regions in the empirical $c(\gamma)$ and $K(q)$ functions. These are associated with discontinuities in the corresponding first or second derivatives. Since there is a formal analogy between thermodynamics and multifractals (see, e.g., Schuster 1988), with $c(\gamma)$ the entropy analog, $K(q)$ the Massieu potential analog, and q^{-1}, the temperature analog, such discontinuities are called "multifractal phase transitions." Scale-breaking mechanisms in deterministic multifractals leading to such transitions have been proposed (e.g., Szépfalusy et al. 1987), but those that are likely relevant here are the two statistical mechanisms recently proposed by Schertzer et al. (1993) and Schertzer and Lovejoy (1994). Both mechanisms depend on finite sample size, and one also depends on the dimension of the observing space.

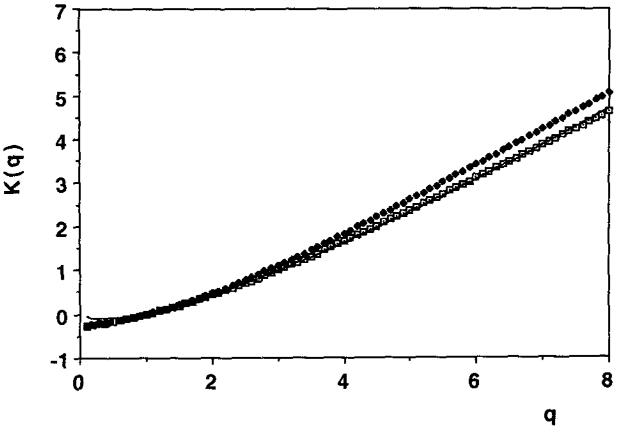

FIG. 10. The $K(q)$ versus q calculated with the regular grid method (empty squares) and with the correlation method (filled diamonds) together with the theoretical curve obtained with the double trace moment technique, i.e., with parameters $\alpha = 0.9$ and $C_1 = 0.3$.

The relation between $K(q)$ and $c(\gamma)$ is given by a Legendre transform [Eq. (5)]. The γ that maximizes $q\gamma - c(\gamma)$ is γ_q and is the solution of $c'(\gamma_q) = q$. Similarly, the value of q that maximizes $q\gamma - K(q)$ is q_γ and is the solution of $K'(q) = \gamma$. There is a one to one correspondence between moments and orders of singularities (see Figs. 11 and 12). Note that if γ is bounded by $\gamma_{\max}$ (which can be γ_S or γ_D) there is a $q_{\max} = c'(\gamma_{\max})$ such that for $q > q_{\max}$, $K(q\gamma) = q\gamma_{\max} - c(\gamma_{\max})$; that is, $K(q)$ becomes linear in q (see Fig. 13).

Consider N_S independent realizations of a multifractal process, each on a space dimension D and each covering a range of scales λ. With more realizations (increasing N_s), a larger and larger portion of the probability space will be explored. Extreme but rare events that were missed with a smaller sample will eventually

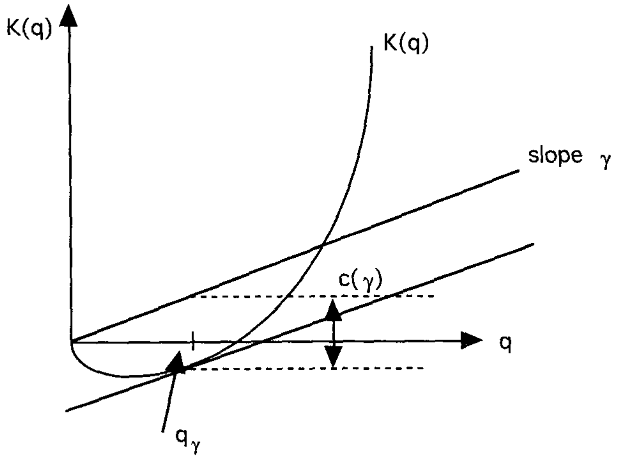

FIG. 11. Graphical construction of the Legendre transform starting from $K(q)$.

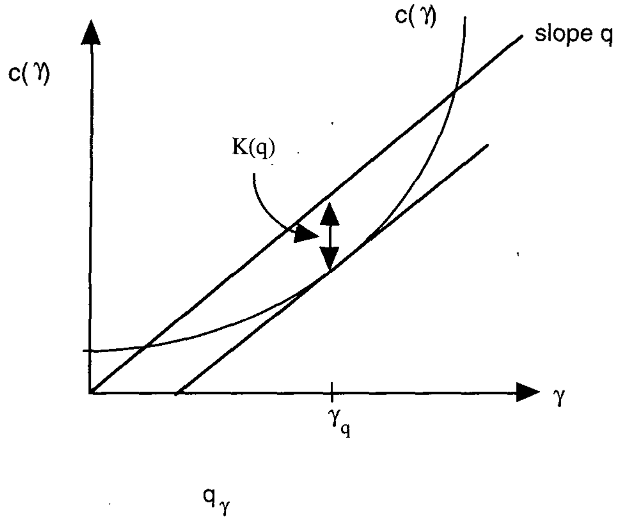

FIG. 12. Graphical construction of the Legendre transform starting from $c(\gamma)$.

be encountered. The extent of the portion of the probability space sampled can be quantified by the sampling dimension D_s (Schertzer and Lovejoy 1989; Lavallée et al. 1991). Using the fact that there are a total of $NN_s = \lambda^{D+D_s}$ structures in the sample, the dimension corresponding to the highest order of singularity likely observed (γ_s) with N_s independent realizations is given by

$$c(\gamma_s) = D + D_s = \Delta_s; \quad D_s \approx \frac{\log N_s}{\log \lambda}, \qquad (12)$$

where Δ_s is the overall effective dimension.

If we now estimate $K(q)$, we must restrict the Legendre transform of $c(\gamma)$ to $\gamma < \gamma_s$, for $q > q_s$; $q_s = c'(\gamma_s)$ and this leads to a spurious linear estimate K_s instead of the nonlinear K; q_s is the maximum moment that can accurately be estimated:

$$K_s(q) = \begin{cases} \gamma_s(q - q_s) + K(q_s), & q \geqslant q_s \\ K(q), & q \leqslant q_s. \end{cases} \qquad (13)$$

This is a second-order phase transition associated with a jump in the second derivative of $K(q)$; $\Delta K''(q_s) = -K''(q_s)$.

To see how first-order transitions can occur, consider Fig. 4, which suggests a discontinuity in $c''(\gamma)$ followed by linear behavior in $c(\gamma)$ for $\gamma > \gamma_D$. This behavior arises when ("bare") multifractal processes proceeding to very small scales are integrated (averaged) over much larger scales. In this case, the resulting "dressed" $c_d(\gamma)$ will display the following second-order transition:

$$c_d(\gamma) = \begin{cases} q_D(\gamma - \gamma_D) + c(\gamma_D), & \gamma \geqslant \gamma_D \\ c(\gamma), & \gamma \leqslant \gamma_D, \end{cases} \qquad (14)$$

where $q_D = c'(\gamma_D)$ and is the absolute slope of the algebraic falloff of the dressed probability distribution; it is the critical order of divergence of statistical moments [$\langle \epsilon^q \rangle = \infty$; $K_d(q) = \infty$, $q \geqslant q_D$]. When $\gamma_s < \gamma_D$, the distinction between the bare and dressed $c(\gamma)$'s is not noticeable, but when the sample size is large enough so that $\gamma_s > \gamma_D$, it is the maximum observable dressed singularity $\gamma_{d,s}$ [it is the solution of $\Delta_S = c_d(\gamma_{d,s})$], which restricts the Legendre transform [not $\Delta_s = c^{-1}(\gamma_s)$]. We thus obtain

$$K_{d,s}(q) = \begin{cases} \gamma_{d,s}(q - q_D) + K(q_D), & q > q_D \\ K(q), & q < q_D, \end{cases} \qquad (15)$$

which is a discontinuity in the first derivative of K.

To obtain more convincing evidence that we really do observe a second-order transition in $c(\gamma)$ [and hence a first-order transition in $K(q)$], we examine more closely one of the histograms that was used in estimating $c(\gamma)$, choosing one that while lying in the scaling region, still has a large number of events associated with it (i.e., it goes to low probability levels; for this figure we used grid elements of approximately 800 km × 800 km). In Fig. 7 we show $\log_{10} \Pr(\rho_\lambda > P)$ versus $\log_{10} P$, where P is the threshold; from the tail behavior, we have a clear indication that $q_D = 3.7 \pm 0.1$, showing that $\gamma_s > \gamma_D$. Indeed, Table 1 indicates that while $\gamma_D \approx 0.6$, $\gamma_{d,s} \approx 0.8$.

7. Double trace moment analysis of the network

We have seen that due to multifractal phase transitions and ill-posed nonlinear regressions, it is difficult to directly estimate the universality parameters from Eqs. (3) or (5). We now turn to a robust technique that estimates C_1, α directly: the double trace moment (DTM) technique (Lavallée et al. 1991; Lavallée et al. 1992). This is done by generalizing the single trace moment by taking the η power of a multifractal field φ_Λ at the largest available scale ratio Λ. Then the q, η double trace moment at resolutions λ and Λ is defined as

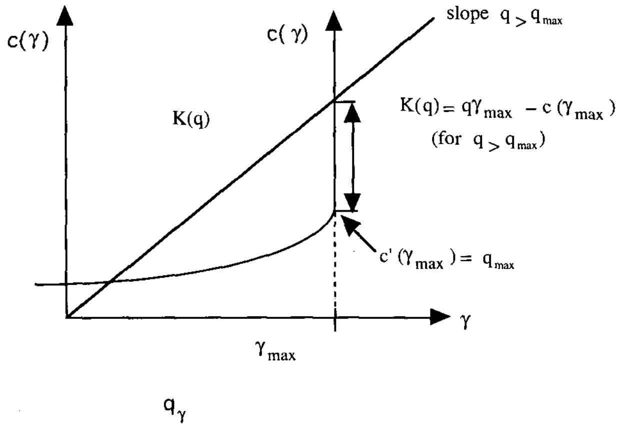

FIG. 13. Graphical construction of the Legendre transform showing the effect of the existence of a maximum order of singularity $\gamma_{\max}$.

TABLE 1. Comparison of parameter estimates from different multifractal estimation techniques.

	PDMS method	Trace moments (grid)	Trace moments (correlation)	Double trace moments (grid, $q = 0.5$)
$\gamma_{\min}$	0.3	0.35	0.26	—
$q_{\min}$	[a]	0.7	0.8	$\approx$0.8[b]
$c(\gamma_{\min})$[c]	0.2	0.3	0.28	—
$\gamma_{d,s}$	0.8	0.7	0.8	—
γ_D	0.6	—	—	—
q_D[d]	3.6	3.5	4.0	$\approx$3[b]
α	—	0.9	1.0	0.9
C_1	—	0.3	0.2	0.3
H	0	[e]	0.1	0.05[f]

[a] The low γ part of the curve is not accurate enough to estimate $q_{\min} = c'(\gamma_{\min})$.

[b] Estimated from the bounds of the linear region of Fig. 15.

[c] Monofractal analyses give $c(\gamma_{\min}) \approx 0.2$.

[d] Direct use of probability distributions (see Fig. 7) gives $q_D \approx 3.7$.

[e] The gridded trace moment cannot estimate H.

[f] The DTM in conjunction with power spectra.

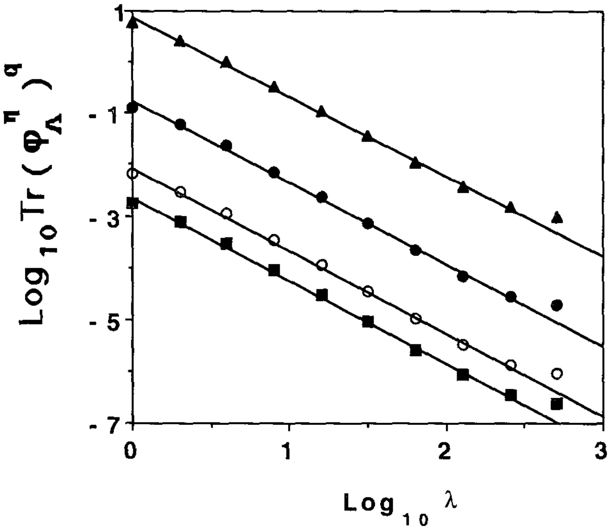

FIG. 14. $\mathrm{Log}[\mathrm{Tr}_\lambda(\varphi_\lambda^\eta)^q]$ versus $\log\lambda$ for several values of η (from top to bottom: $\eta = 1.2, 0.7, 0.3, 0.1$) for the network. We used $q = 2$ and the scale ratio $\lambda = 1$ for a distance of 20 000 km.

$$\mathrm{Tr}_\lambda(\varphi_\lambda^\eta)^q = \left\langle \sum_i \left(\int_{B_{\lambda,i}} \varphi_\Lambda^\eta d^D x \right)^q \right\rangle \propto \lambda^{K(q,\eta)-(q-1)D}, \tag{16}$$

where the sum is over all the λ resolution boxes $B_{\lambda,i}$ (dimension D) required to cover the multifractal, $K(q, \eta)$ is the (double) scaling exponent, and $K(q, 1)$ is the usual scaling exponent. Although it looks complicated, applying Eq. (16) to the field of interest simply consists of taking various powers η of the field at its highest resolution (Λ), then degrading the result to a lower resolution (λ), finally averaging the qth power of the result.

The scaling exponent $K(q, \eta)$ satisfies the following relation:

$$K(q, \eta) = K(q, \eta) - qK(\eta, 1), \tag{17}$$

where the term $qK(\eta, 1)$ arises due to the normalization. The DTM is useful for universal multifractals since, in that case, we obtain the simple relation:

$$K(q, \eta) = \eta^\alpha K(q, 1), \tag{18}$$

which can readily be used to estimate α by fixing q and varying η.

The first step in applying the DTM technique is to check the scaling range of various moments. Figure 14 shows $\log\mathrm{Tr}[(\varphi_\lambda^\eta)^q]$ versus $\log\lambda$ for $q = 2$. We used a 512 × 512 regular grid (sinusoidal projection) to analyze the density of stations. As we can see, scaling is observed for $\log\mathrm{Tr}[(\varphi_\lambda^\eta)^q]$ versus $\log\lambda$ (for different values of q, $\eta = 1$) in the range $0 \leqslant \log\lambda \leqslant 2.0$, which, as expected, is the same as that deduced from Fig. 5. From these curves we have a plot $\log|K(q, \eta)|$ versus $\log\eta$ and obtain α, C_1 by linear regression over the power-law region of the double trace moment that we show on Fig. 15: $\alpha = 0.9 \pm 0.2$ and $C_1 = 0.3 \pm 0.1$.

Due to the phase transitions Eq. (5), hence (18), breaks down for low and high η, specifically for $\min(\eta, q\eta) < q_{\min}$ and $\max(\eta, q\eta) > q_D$, respectively (since $q = 2.0$ here for $\eta \approx {<}0.3$, and $\eta \approx {>}1.8$). To gain more confidence in these results, on the same figure we have plotted the result of the analysis for a simulated field using the estimated parameters with an infinite number of stations (the straight line) and a simulated network consisting of only a finite number (7077 stations) generated from a simulated density field (details of which

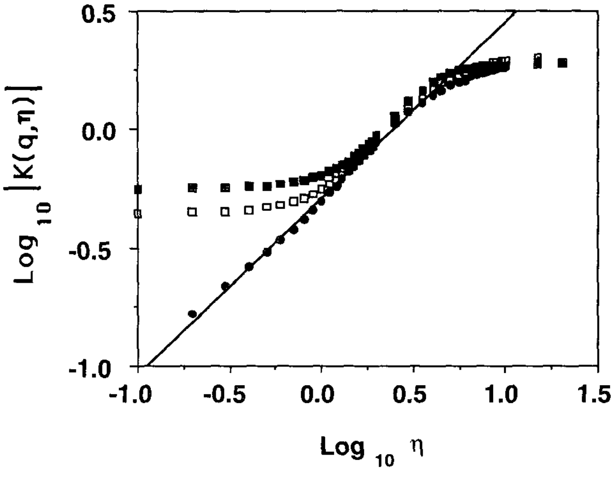

FIG. 15. $\mathrm{Log}|K(q, \eta)|$ versus $\log\eta$ for the network (filled squares), a field (without any minimum thresholding) having the same parameters as the network (filled circles), and a simulated network obtained from the simulated field (empty squares).

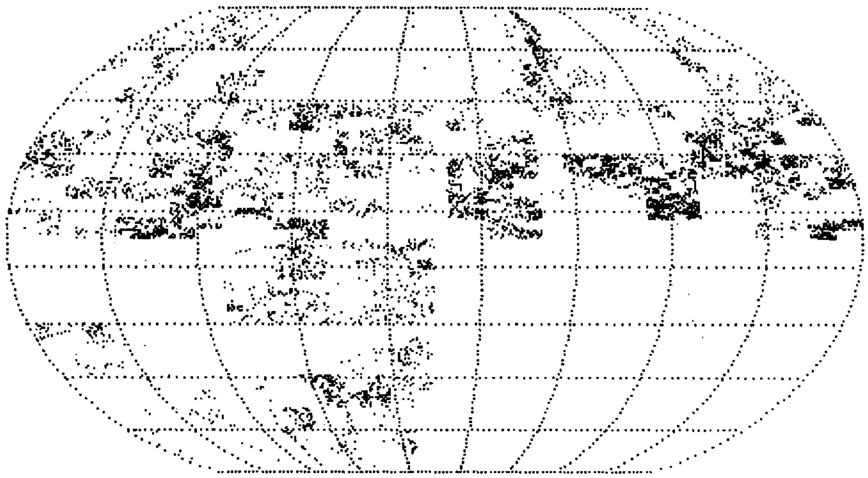

FIG. 16. Position of the 7077 stations for the simulated network used for testing the different analysis methods.

are given in the next section). Whereas the large η behavior is well reproduced from the model simply due to the fact that it is a unique realization (yielding a second-order high phase transition), the finite number of stations clearly gives rise to a low phase transition with very nearly the same transition point as for the data.

We can now use the DTM results to estimate the final universal multifractal parameter H. We mentioned that one of the basic ingredients of multifractal processes is the presence of a quantity that is conserved from one scale to the next. There is no a priori reason to think that the density field has such properties but we can introduce a field φ_λ that has the conservation property $\langle \varphi_\lambda \rangle$ is constant (independent of scale). The density field (ρ_λ) is related to this field by

$$\rho_\lambda = \varphi_\lambda^a \lambda^{-H}. \qquad (19)$$

No theory tells us which field is φ_λ or the corresponding value of a; however, changing a will simply give us a different but equivalent representation of the conserved multifractal process. Therefore H is a measure of nonconservation of the field. It specifies the order of fractional integration required to obtain ρ_λ from φ_λ. For a self-similar (isotropic) scaling process, the energy (power) spectrum $E(k)$ for wavenumber k is of the form $E(k) \approx k^{-\beta}$, with spectral exponent β, that is, it is also linear in a log–log plot. The DTM is insensitive to the value of H as long as β is less than that of a conserved process [i.e., $\beta < 1 - K(2)$, see Lavallée (1991), Lavallée et al. (1993) for a discussion]. To evaluate the parameter H, we used the estimate of α and C_1 from the DTM, and the order of fractional integration needed to obtain the nonconserved process from the conserved one is given by

$$H = \frac{\beta - 1 + K(2)}{2} = \frac{\beta - 1}{2} + \frac{C_1(2^\alpha - 2)}{2(\alpha - 1)}. \qquad (20)$$

Since the field for the density of stations is distributed on a sphere, we should really use a decomposition into spherical harmonics rather than Fourier analysis; however, for simplicity, we performed the analysis on equal area projections of portions of the earth and use standard spectra. For each projection we generated 10 maps of 8000 km × 8000 km sections of the earth (five in the Northern Hemisphere and five in the southern) centered 72° of longitude apart. We then calculated the power spectrum from this ensemble. For the range of scales greater than or equal to 200 km, we estimated the spectral slope $\beta \approx 0.63 \pm 0.13$. Using this value in conjunction with $\alpha = 0.9 \pm 0.2$ and $C_1 = 0.3 \pm 0.1$ and with Eq. (20), we obtain $H \approx 0.05 \pm 0.1$.

8. Simulation of the network

In the previous section we presented some results for a simulated network. This simulation was mainly used to test the different methods and to verify our understanding of the different techniques; particularly of concern are the inner limit of the scaling, the minimum order of singularity associated with the finite number of stations, and the accuracy of the estimates of the universal multifractal parameters. In this section we will present some more details on the method used to produce the simulation and some further results. We show an example of a simulated network in Fig. 16.

The simulations were performed using a discrete cascade (Schertzer and Lovejoy 1987) on a 256 × 256 grid [this is roughly the observed range of scaling found empirically for the network (see Fig. 14), approximately 200 to 20 000 km]. The discreteness (only factors of 2 in scale are used) accounts for the appearance of unrealistic straight line structures; since this work was performed, Pecknold et al. (1993) have shown how to extend continuous cascades to the case $\alpha < 1$, but the

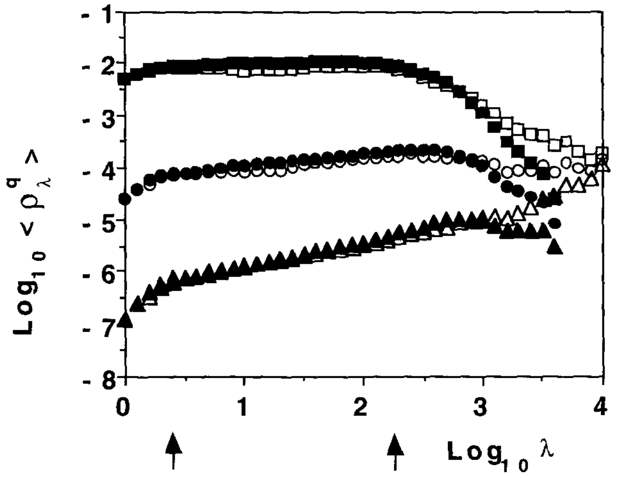

FIG. 17. Log of the statistical moments against logλ using the correlation method for the real network (empty symbols) and for the simulated network (filled symbols) for q = 0.5 (squares), q = 1.0 (circles), and q = 1.5 (triangles). The arrows indicate the expected scaling region.

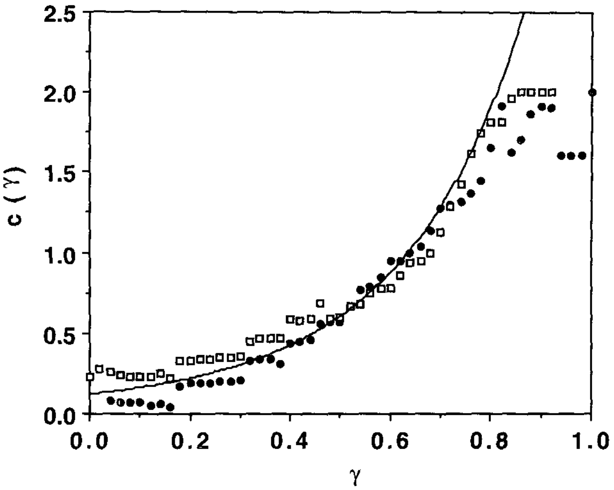

FIG. 18. The $c(\gamma)$ versus γ for the real network (filled circles) and for the simulated network (empty squares). The solid line is the theoretical curve for the $K(q)$ function using the parameters determined by the double trace method, i.e., α = 0.9 and C_1 = 0.3.

statistics of interest here will be essentially the same. The field produced by the simulation with the parameters deduced by the DTM method was taken as the density field. We multiplied this field by the expected total number of stations N_{TOT} in order to obtain a simulated network with a total number of stations near to that observed. With the same total number of stations we should be able to reproduce roughly the same $\gamma_{\min}$ as the real network since $\gamma_{\min} \approx \log \rho_{\lambda\,\min}/\log\lambda$ (in particular, low values $N_{\text{TOT}}\,\rho_\lambda < 0.5$ were set to zero). We rounded the number of stations in each box to the nearest integer value. Within each box we then distributed the number of stations according to a uniform random distribution and then extracted a database with the same resolution as the real network. Note that both the total scaling range as well as the total number of stations are important parameters in the simulation.

We estimated the usual statistical moments using both the regular grid and the correlation estimates of the trace moments (Fig. 17). The simulation is in very good agreement with the scaling properties of the real network. We were even able to reproduce the scaling break due to the finite number of stations (introducing the homogeneity scale) confirming that it really is the limited number of stations that is responsible for the break. Figure 18 shows the $c(\gamma)$ curve obtained by the PDMS method. Here again the empirical and simulated curves are in good agreement. From the statistical moments on a regular grid of Fig. 17 we produced the $K(q)$ curve for both networks (Fig. 19). We can see that except for small differences for large q, both curves fall on top of one another. It is also the case for the DTM technique shown in the previous section (Fig. 15). The departure from the theoretical curve is due to the finite number of stations that result in a minimum value of q and γ where the analysis is valid (as discussed in previous sections). The simulations indicate a $q_{\min}$ close to that observed showing that this feature can also be explained by the finite number of stations. As a final note, the simulation did not have the same q_D; hence the phase transition in the simulation at large q is due to q_s, not q_D.

9. Conclusions

The estimation of geophysical fields from inhomogeneous geophysical networks has always been a difficult problem. The techniques required to solve the

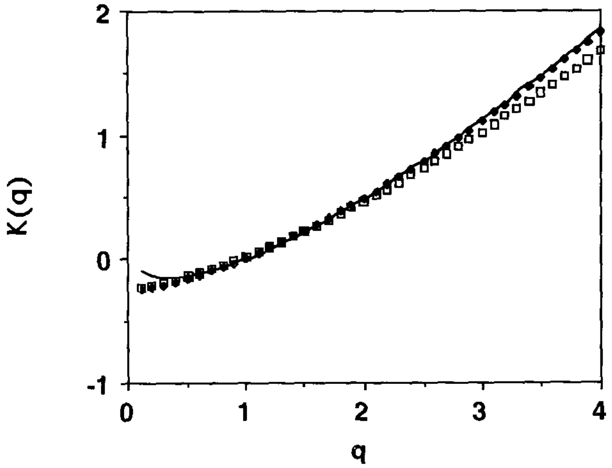

FIG. 19. The $K(q)$ versus q for a simulated network of 7077 stations having parameters α = 0.9 and C_1 = 0.3 (diamonds) and the same function for the real network (empty squares). We also show the theoretical curve for α = 0.9 and C_1 = 0.3.

problem depend critically on the statistical assumptions that are made about the network, particularly its behavior as a function of scale and as a function of the density of the network at a given scale. Since a priori there is no length scale associated with the process that produced the network, the simplest (and in the absence of other information, the only) assumption possible is that it is scaling. Early scaling attempts treated the problem by considering the location of stations as a geometric set of points with fractal properties. Here we propose an approach based on the density of stations, which is a scaling field; hence it is multifractal (i.e., the scaling of the high- and low-density regions are different). We empirically verify this for the global rain gauge network using a series of analysis techniques over the range of scales of approximately 200–20 000 km. First, the probability distribution/multiple scaling and then trace moments techniques are applied, the latter both with a grid and using a new technique without a grid (a "correlation method"). We find that qualitative changes occur first for low-density regions (due to the finite number of stations) and, second, at the high-density regions, where a new "hard" multifractal behavior is observed. These qualitative changes in the scaling exponents (which we find occur at $q_{\min} \approx 0.7$, and $q_D \approx 3.6$) are "multifractal phase transitions." We also apply the double trace moment technique to argue that the density is a universal multifractal—the generic result of a scaling nonlinear process. This method, combined with spectral analysis, allows us to estimate the three universal multifractal parameters: $\alpha = 0.9 \pm 0.2$, $C_1 = 0.3 \pm 0.1$, and $H = 0.05 \pm 0.1$. Finally, by numerically simulating a network with these parameters, we quantitatively showed that both the finite range of scaling, as well as the low-density phase transition, were the results of the finite number of stations.

The multifractal character of geophysical networks is important since many geophysical fields have already been found to be multifractal, and others are likely to be. If this is true, then the densities of these fields estimated from the network are simply the product of the true field values and the station density; correcting for the bias ("multifractal objective analysis") is reduced to the problem of the product of multifractals. Some attempts to solve this problem have been made by Tessier (1993), Tessier et al. (1993a), and Salvadori et al. 1994, and will be detailed in future publications.

APPENDIX

The Anisotropy of the Network

To quantify the anisotropy in the scaling of the measuring network, we partitioned the axis of the globe into slices of equal z (where z is the length of the projection of the slice onto the axis that goes from the center of the earth to the North Pole) so that the area of the intersection of each slice with the earth's surface will be the same. We partition the earth in such a fashion because we need to perform the analysis on one-dimensional intersections of the original set. The codimensions are invariant under intersection, so that corresponding dimensions will simply be reduced by 1. In contrast, taking one-dimensional projections (i.e., just considering the latitudes of stations irrespective of longitude) will have dimension (since the measuring stations have dimension greater than 1) and hence will be uninteresting. We performed a regular box-counting analysis on each slice using the definition of distance that $L = |\theta_1 - \theta_2|$ and then we averaged the $N(L)$ value for all slices. We then rotated the coordinate system and performed the same analysis in the other direction. For both analyses the results are shown in Fig. A1. It can be seen that there is a small anisotropy in the measuring network since the fractal dimension calculated in the north–south and in the east–west direction is, respectively, 0.85 and 0.77. The anisotropy of the network could further be characterized by the use of the elliptical dimension D_{el} (Lovejoy et al. 1987; Schertzer and Lovejoy 1985, 1987), which in this case is given by

$$D_{\mathrm{el}} = 1 + \frac{C_{\mathrm{N-S}}}{C_{\mathrm{E-W}}} = 1 + \frac{0.185 \pm 0.0035}{0.23 \pm 0.005} = 1.70 \pm 0.06, \quad \text{(A1)}$$

where $C_{\mathrm{N-S}}$ and $C_{\mathrm{E-W}}$ are the codimension in the north–south and east–west directions, respectively; the codimension is the difference between the dimension of the embedding space (in our case 1.0) and the fractal dimension. If the network was isotropic we would have obtained $D_{\mathrm{el}} = 2.0$. The accuracy of D_{el} is evaluated by assuming an accuracy of 1% on individual points from which we evaluated a minimum χ^2 line.

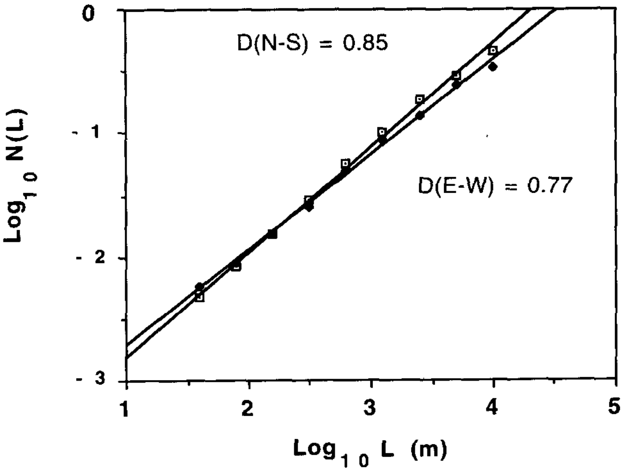

FIG. A1. Log of the number of pairs of stations divided by the total number of boxes within a certain "slice" averaged over all slices against the log of the distance for north–south-oriented slices (empty squares) and east-west-oriented slices (filled diamonds).

Acknowledgments. We thank P. Hubert, J. P. Carbonnel, C. Hooge, J. F. Malouin, F. Francis, F. Schmitt, and P. Ladoy for helpful comments.

REFERENCES

Bell, T. H., 1975: Statistical features of sea floor topography. *Deep-Sea Res.*, **22**, 883–891.

Brax, P., and R. Pechanski, 1991: Levy stable law description on intermittent behaviour and quark-gluon plasma phase transitions. *Phys. Lett. B*, **253**, 225–230.

Chigirinskaya, Y., D. Schertzer, S. Lovejoy, A. Lazarev, and A. Ordanovich, 1994: Unified multifractal atmospheric dynamics tested in the tropics. Part 1: Horizontal scaling and self-organized criticality. *Nonlinear Processes in Geophysics*, in press.

Francis, F., T. Falco, S. Lovejoy, D. Schertzer, B. Kerman, and M. Drinkwater, 1994: Scale invariance and universal multifractals in sea ice synthetic aperture radar reflectivity fields. *J. Geophys. Res.*, submitted.

Gabriel, P., S. Lovejoy, D. Schertzer, and G. Austin, 1988: Multifractal analysis of resolution dependence in satellite imagery. *J. Geophys. Res.*, **15**, 1373–1376.

Grassberger, P., 1983: Generalized dimensions of strange attractors. *Phys. Lett. A*, **97**, 227–230.

Griffiths, P., and I. D. Hill, 1985: *Applied Statistics Algorithms*, Ellis Horwood Limited, 410 pp.

Gupta, V. K., and E. Waymire, 1990: Multiscaling properties of spatial rainfall and river distribution. *J. Geophys. Res.*, **95**(3), 1999–2010.

Halsey, T. C., M. H. Jensen, L. P. Kadanoff, I. Procaccia, and B. Shraiman, 1986: Fractal measures and their singularities: The characterization of strange sets. *Phys. Rev. A*, **33**, 1141–1151.

Hentschel, H. G. E., and I. Proccacia, 1983: The infinite number of generalized dimensions of fractals and strange attractors. *Physica*, **8**, 435–444.

Kolmogorov, A. N., 1962: A refinement of previous hypotheses concerning the local structure of turbulence in viscous incompressible fluid at high Reynolds number. *J. Fluid Mech.*, **83**, 349.

Korvin, G., 1992: *Fractal Models in the Earth Sciences*, Elsevier, 396 pp.

——, D. M. Boyd, R. O'Dowd, 1990: Fractal characterisation of the south Australian gravity station network. *Geophys. J. Int.*, **100**, 535–539.

Lavallée, D., S. Lovejoy, and D. Schertzer, 1991: On the determination of the codimension function. *Non-Linear Variability in Geophysics: Scaling and Fractals*, D. Schertzer, and S. Lovejoy, Eds., Kluwer, 99–110.

——, ——, ——, and F. Schmitt, 1992: On the determination of universal multifractal parameters in turbulence. *Topological Aspects of the Dynamics of Fluids and Plasmas*, K. Moffat, M. Tabor, and G. Zalslavshy, Eds., Kluwer, 463–478.

——, ——, ——, and Ph. Ladoy, 1993: Nonlinear variability and landscape topography: Analysis and simulation. *Fractals in Geography*, L. De Cola, and N. Lam, Eds., Prentice-Hall, 171–205.

Lazarev, A., D. Schertzer, S. Lovejoy, and Y. Chigirinskaya, 1994: Unified multifractal atmospheric dynamics tested in the tropics. Part 2: Vertical scaling and generalized scale invariance. *Nonlinear Processes in Geophysics*, in press.

Lovejoy, S., and D. Schertzer, 1986: Scale invariance, symmetries, fractals and stochastic simulations of atmospheric phenomena. *Bull. Amer. Meteor. Soc.*, **67**, 21–32.

——, and ——, 1988: Extreme variability, scaling and fractals in remote sensing: Analysis and simulation. *Digital Image Processing in Remote Sensing*, J. P. Muller, Ed., Francis and Taylor, 177–212.

——, and ——, 1990: Multifractals, universality classes and satellite and radar measurements of cloud and rain fields. *J. Geophys. Res.*, **95**, 2021–2034.

——, and ——, 1991: Multifractal analysis techniques and the rain and cloud fields from 10^{-1} to 106 m. *Non-Linear Variability in Geophysics: Scaling and Fractals*, D. Schertzer and S. Lovejoy, Eds., Kluwer, 111–144.

——, ——, and P. Ladoy, 1986a: Fractal characterisation of inhomogeneous measuring networks. *Nature*, **319**, 43–44.

——, ——, and ——, 1986b: Brighter outlook for weather forecasts. *Nature*, **320**, 401.

——, ——, and A. A. Tsonis, 1987: Functional box-counting and multiple dimensions in rain. *Science*, **235**, 1036–1038.

Mandelbrot, B., 1967: How long is the coastline of Britain? Statistical self-similarity and fractional dimension. *Science*, **155**, 636–638.

——, 1974: Intermittent turbulence in self-similar cascades: Divergence of high moments and dimension of the carrier. *J. Fluid Mech.*, **62**, 331–350.

——, 1975: Stochastic models for the earth's relief, the shape and the fractal dimension of the coastlines, and the number-area rule for islands. *Proc. Natl. Acad. Sci. USA*, **72**, 3825–3828.

Meneveau, C., and K. R. Sreenevasan, 1987: Simple multifractal cascade model for fully developed turbulence. *Phys. Rev. Lett.*, **59**(13), 1424–1427.

Montariol, F., and R. Giraud, 1986: Analyse fractale du réseau météorologique. Rapport, Météorologie Nationale, Paris, France, 77 pp.

Nicolis, C., 1993: Optimizing the global observational network: A dynamical approach. *J. Appl. Meteor.*, **33**, 1751–1759.

Parisi, G., and U. Frisch, 1985: A multifractal model of intermittency. *Turbulence and Predictability in Geophysical Fluid Dynamics and Climate Dynamics*, M. Ghil, R. Benzi, and G. Parisi, Eds., North Holland, 84–88.

Pecknold, S., S. Lovejoy, D. Schertzer, C. Hodge, and J. F. Malouin, 1993: The simulation of universal multifractals. *Cellular Automata: Prospects in Astrophysical Applications*, J. M. Perdang and A. LeJeune, Eds., World Scientific, 228–267.

Pflug, K., S. Lovejoy, and D. Schertzer, 1991: Generalized scale invariance, differential rotation and cloud texture. *Nonlinear Dynamics of Structures*, R. Z. Sagdeev, U. Frisch, A. S. Moiseev, and A. Erokhin, Eds., World Scientific, 72–78.

——, ——, and ——, 1993: Generalized scale invariance, differential rotation and cloud texture. *J. Atmos. Sci.*, **50**, 538–553.

Press, W. H., B. P. Flannery, S. A. Teukolsky, and W. T. Vetterling, 1992: *Numerical Recipes in C, The Art of Scientific Computing*, 2d ed, Cambridge University Press, 994 pp.

Richardson, L. F., 1961: The problem of contiguity: An appendix of statistics of deadly quarrels. *General Systems Yearbook*, **6**, 139–187.

Salvadori, G. S., P. Ratti, G. Belli, S. Lovejoy, and D. Schertzer, 1994: Multifractal and Fourier analysis of Seveso pollution. *J. Toxicol. Environ. Chem.*, in press.

Schertzer, D., and S. Lovejoy, 1983: The dimension of atmospheric motions. Preprints, *IUTAM Symp. on Turbulence and Chaotic Phenomena in Fluids*, Tokyo, Japan, 141–144.

——, and ——, 1984: On the dimension of atmospheric motions. *Turbulence and Chaotic Phenomena in Fluids, IUTAM*, T. Tatsumi, Ed., Elsevier Science Publishers, 505–512.

——, and ——, 1985: Generalized scale invariance, differential rotation and cloud texture. *Turbulent Shear Flow 4*, B. Launder, Ed., Springer-Verlag, 7–33.

——, and ——, 1987: Physical modeling and analysis of rain and clouds by anisotropic scaling of multiplicative processes. *J. Geophys. Res. D*, **92**(8), 9693–9714.

——, and ——, 1989: Nonlinear variability in geophysics: Multifractal analysis and simulation. *Fractals: Physical Origin and Consequences*, L. Pietronero, Ed., Plenum, 49.

——, and ——, 1991: Nonlinear geodynamical variability: Multiple singularities, universality and observables. *Non-Linear Variability in Geophysics: Scaling and Fratals*, D. Schertzer and S. Lovejoy, Eds., Kluwer, 41–82.

——, and ——, 1994: Multifractal generation of self-organized criticality. *Fractals in the Natural and Applied Sciences*, M. M. Novak, Ed., Elsevier, 325–339.

——, ——, and D. Lavallee, 1993: Generic multifractal phase transitions and self-organized criticality. *Cellular Automata: Prospects in Astrophysical Applications,* J. M. Perdang and A. Lejeune, Eds., World Scientific, 216–227.

Schmitt, F., S. Lovejoy, D. Schertzer, D. Lavallée, and C. Hooge, 1992a: First estimates of multifractal indices for velocity and temperature fields. *C. Roy. Acad. Sci. Paris, Ser. II,* **314,** 749–754.

——, D. L. D. Schertzer, and S. Lovejoy, 1992b: Empirical determination of universal multifractal exponents in turbulent velocity fields. *Phys. Rev. Lett.,* **68,** 305–308.

——, ——, S. Lovejoy, and Y. Brunet, 1994: Estimation of universal multifractal indices for atmospheric turbulent velocity fields. *Fractals,* **3,** 568–575.

Schuster, H. G., 1988: *Deterministic Chaos 2.* Rev. ed. VCH, 220 pp.

Szépfalusy, P., T. Tél, A. Csordas, and Z. Kovas, 1987: Phase transitions associated with dynamical properties of chaotic systems. *Phys. Rev. A,* **36,** 3525–3528.

Tessier, Y., 1993: Multifractal objective analysis, rain and clouds. Ph.D. thesis, McGill University, 138 pp.

——, S. Lovejoy, and D. Schertzer, 1993a: Universal multifractals: Theory and observations for rain and clouds. *J. Appl. Meteor.,* **32,** 223–250.

——, ——, ——, D. Lavallée, and B. Kerman, 1993b: Universal multifractal indices for the ocean surface at far red wavelengths. *Geophys. Res. Lett.,* **20**(12), 1167–1170.

Venig-Meinesz, F. A., 1951: A remarkable feature of the Earth's topography. *Proc. K. Ned. Akad. Wet., Ser. B: Phys. Sci.,* **54,** 212–228.

Yaglom, A. M., 1966: The influence on the fluctuation in energy dissipation on the shape of turbulent characteristics in the inertial interval. *Sov. Phys. Dokl.,* **2,** 26–30.